

Manipulation of Majorana Modes in a Double Quantum Dot

Jesus D. Cifuentes¹ and Luis G. G. V. Dias da Silva¹

¹*Instituto de Física, Universidade de São Paulo, C.P. 66318, 05315-970 São Paulo, SP, Brazil*

(Dated: December 14, 2018)

(To be written)

I. INTRODUCTION

In the last few decades the interest in the so called Majorana fermions has been increasing. The particle proposed by the physicist Ettore Majorana as the real field solution of the Dirac equation describes a fermion which is its own antiparticle, hence it has no charge nor mass. To the date no fundamental particle with these characteristics has been found. However, theoretical research predicts that Majorana Fermions emerge as quasi-particles at the boundary of certain topological superconductors. Kitaev¹ Recently, the new technological innovations allowed the observation of Majorana signatures in different topological materials.²⁻⁵

Despite the positive experimental results, their is still certain skepticism about the existence of Majorana Fermions. One of the reasons is that some properties of Majorana quasiparticles like the expected non-abelian statistics have not been measure. This property is of especial interest due to its promising applications in topological quantum computing. The braiding protocol based on Majorana's non-abelian statistics is the key to fault-tolerant quantum computation.^{6,7}

A promising method to detect Majorana modes consists in attaching a quantum dot (QD) to the edges of a Majorana chain in the topological phase and executing transport measurements through the QD.⁸ The Majorana mode at the end of the chain then leaks inside the QD⁹ which produces a zero-bias conductance peak of half a quanta $\frac{e^2}{2h}$ through the dot. This is a Majorana signature which produces half of the expected peak by a regular fermion. Recently, experiments including hybrid Majorana-QD systems have been performed.¹⁰ In addition, the similarity of this phenomenon with the Kondo effect, where the zero-bias conductance peak takes $\frac{e^2}{h}$, motivated the study of combined Kondo-Majorana physics in this system.^{11,12} This project revealed the existence of a region of parameters where both, Kondo and Majorana physics, coexist.

This idea has turned on new lights into the design of quantum architectures,^{13,14} because today's precise experimental control over the parameters of QDs - energy levels, tunneling couplings, etc. - offers the unique possibility of manipulating the Majorana modes inside multi-dot systems. The simplest case where Majorana manipulation is possible is in a double quantum dot. So far, no complete analysis of this simple case has been done. The goal of this project is to fill this gap by realizing a full quantum transport study of the effects of coupling

a Majorana mode with a double quantum dot. By tuning the QD gate voltages and the Majorana couplings we will be able to probe the mobility of the Majorana modes through the dots.

We considered both interacting and non-interacting cases. For interacting systems we used a obtained the exact transport description. On non-interacting models we used a NRG approach. We found that in symmetric couplings In the non-interacting case, we confirmed that shifting the QDs gate voltage induces the Majorana to tunnel only to the other dot. In addition, an indirect coupling of the second dot could cause destructive interference with the Majorana signature. In the interacting case, the NRG simulations confirmed these results and showed that other interacting effects - like Kondo and RKKY¹⁵⁻¹⁷ - could coexist with the Majorana signatures. On the other hand, when only one QD is coupled to the leads and the other Dot is attached to the QD, the Kondo effect is annihilated due to the destructive interference generated by extra dot¹⁸. Our study includes how the Majorana mode interacts with these two effects.

II. MODEL AND METHODS

We consider the setup shown in Figure 5 in which a Majorana Bound State (MBS) at the edge of Topological Superconductor(TS) is coupled to a double quantum dot (DQD), which is attached to a single metallic lead. The Hamiltonian of this system can be partitioned in four terms: the DQD Hamiltonian H_{DQD} , the Lead Hamiltonian H_{Lead} , the DQD-lead interaction $H_{DQD-Lead}$ and the coupling between the DQD and the Majorana mode H_{M-DQDs} and

$$H = H_{DQD} + H_{Lead} + H_{DQD-Lead} + H_{M-DQDs} \quad (1)$$

The interacting Anderson Model describes the DQD-lead system

$$H_{DQD} = \sum_{i \in \{1,2\}} \sum_{\sigma \in \{\downarrow, \uparrow\}} \left(\epsilon_{di} + \frac{U_i}{2} \right) \hat{n}_{i\sigma} + \frac{U_i}{2} (\sum_{\sigma} \hat{n}_{i\sigma} - 1)^2 \\ + \sum_{\sigma \in \{\uparrow, \downarrow\}} t_{dots} (d_{1\sigma}^\dagger d_{2\sigma} + d_{2\sigma}^\dagger d_{1\sigma}), \quad (2)$$



FIG. 1: DQD-Majorana set-up. Solid lines: standard coupling. Dashed lines: Majorana spin- \downarrow effective couplings (6). The atomic energy levels appear inside each QD. Red dashed horizontal lines represent the Fermi level.

and

$$H_{Lead} = \sum_{\mathbf{k}\sigma} \epsilon_{\mathbf{k}} c_{\mathbf{k}\sigma}^\dagger c_{\mathbf{k}\sigma} \quad (3)$$

$$H_{DQD-Lead} = \sum_{\mathbf{k}\sigma} \sum_{i \in \{1,2\}} V_{i\mathbf{k}} c_{\mathbf{k}\sigma}^\dagger d_{i\sigma} + V_{i\mathbf{k}}^* d_{i\sigma}^\dagger c_{\mathbf{k}\sigma}, \quad (4)$$

where ϵ_{di} is the energy level of dot i , U_i is the Coulomb repulsion and t_{dots} is the coupling parameter between both QDs. The operator $d_{i\sigma}^\dagger$ creates a particle in dot i with spin σ and $\hat{n}_{i\sigma} := d_{i\sigma}^\dagger d_{i\sigma}$ is the particle number operator of state i . $c_{\mathbf{k}\sigma}^\dagger$ is the creation operator a particle with momentum \mathbf{k} and spin σ in the lead. $\epsilon_{\mathbf{k}l}$ is the corresponding energy and $V_i(\mathbf{k})$ describes the tunneling coupling between the lead and dot i .

The Majorana modes are modeled as a superposition of the creation and annihilation operators of a spin \downarrow particle f_\downarrow

$$\gamma_1 := \frac{1}{\sqrt{2}} (f_\downarrow^\dagger + f_\downarrow), \gamma_2 := \frac{i}{\sqrt{2}} (f_\downarrow^\dagger - f_\downarrow). \quad (5)$$

This makes possible to define an effective coupling between the Majorana Mode and the DQD by attaching γ_1 with the spin- \downarrow channel in the QDs

$$H_{M-DQD} = \sum_{i=1}^2 t_i (d_{i\downarrow}^\dagger \gamma_1 + \gamma_1 d_{i\downarrow}) + \epsilon_M \gamma_1 \gamma_2. \quad (6)$$

where t_i is the coupling parameter between the Majorana mode and QD i . ϵ_m is the coupling energy between both Majorana modes. This effective model is able to reproduce the physical effects of more elaborated couplings¹² such

Ruiz-Tijerina *et al.* showed that this effective coupling is able to reproduce effectively the transport effects of the Kitaev chain in the topological phase is attached to a single QD.

A. Methods

B. Non-interacting case

To study the non-interacting case ($U = 0$), we use Zubarev's ballistic transport approach¹⁹ to compute the Green functions associated to both quantum dot operators ($G_{d_1 d_1^\dagger}(\omega), G_{d_2 d_2^\dagger}(\omega)$). The detailed procedure is included in Appendix A. The transport equations define a linear system where the Hamiltonian parameters ($t_1, t_2, \epsilon_1 \dots$) and the energy ω are taken as fix variables. The flow graph in FIG.2 depicts the linear map associated to the transport in an hybrid Majorana-DQD system (see (A6)). The energies of each operator are located at the center of the vertexes while the vertex couplings represent the off-diagonal terms. The Majorana mode connects two regions of the graph, both of them representing a DQD. The upper DQD is conformed by annihilation operators while the lower one is formed by creation operators. The couplings in the lower part are the upper parameters multiplied by -1 .

To simplify the solution of this system we used a graph linear algorithm that speeds-up the process of Gauss-Jordan elimination.²⁰ Starting with the flow graph at FIG.2 (a), the algorithm successively "pops" the vertexes till only one vertex remains in the the graph. Popping a vertex must be understood as the Gaussian elimination of the line and the column in the transport matrix containing that vertex (see Section A). This modifies the energies of the vertexes and the coupling parameters. Changing the order of elimination of the vertexes could lead to different equivalent representations of the final polynomial. Finding a suitable elimination order could significantly reduce the complexity of the solution²⁰.

This graph-linear solver algorithm turns out to be particularly good for Majorana systems since the Majorana fermion is a natural cutting point that divides the graph in two sections. This allows us to exploit the graph structure to simplify the solution of the system by selecting a suitable order of vertex-elimination. Fig.2 depicts this process. In the first step (a) to (b), we pop consecutively the vertexes $c_{k,\downarrow}, c_{k,\downarrow}^\dagger, d_{2,\downarrow}, d_{2,\downarrow}^\dagger$. The new parameters ϵ_{DQD}^\pm , M_2 and T_\pm (See (A)) are functions of $\epsilon_1, \epsilon_2, t_1, t_2$, etc. These functions gather the transport information through the popped vertexes. The next step is to pop vertexes $d_{1,\downarrow}^\dagger$ and f_\downarrow , which condensed the transport information of the whole system into the remaining vertex $d_{1,\downarrow}$. As shown in section A the energy of vertex $d_{1,\downarrow}$ is $\omega - G_{d_{1\downarrow} d_{1\downarrow}^\dagger}(\omega)$, hence giving a very compact expression for the Green function

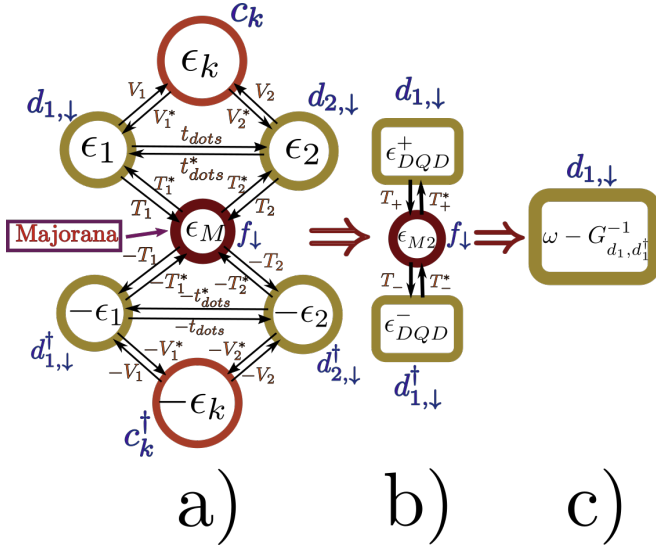


FIG. 2: Transport flow in a DQD Majorana system.

$$G_{d1, d1^\dagger}(\omega) = \frac{1}{\omega - \epsilon_{DQD}^+ - \frac{\|T_+\|^2}{\omega - \epsilon_{M2} - \frac{\|T_-\|^2}{\epsilon_{DQD}^-}}}. \quad (7)$$

The final result will depend on the broadening parameter of QD i with the lead (Γ_i). This broadening satisfies the equation

$$-i\Gamma_i = \lim_{s \rightarrow 0} \sum_{\mathbf{k}} \frac{V_i^* V_i}{\omega + is - \epsilon_k}. \quad (8)$$

By convention we will take Γ_1 as the energy unit for the rest of the project. Finally we compute the DOS

$$\rho_{1\sigma}(\omega) = -\frac{1}{\pi} \text{Im} \left[G_{d1\sigma, d1\sigma}(\omega) \right]. \quad (9)$$

Similar results can be obtain for the DOS of the second $\rho_{2\sigma}$. Comparing these results for both dots at the Fermi energy we will be able to determine which dot exhibits a Majorana signature.

C. Interacting case (NRG)

For the interacting case, we used the Numerical Renormalization Group (NRG) approach^{21–23}. The algorithm assumes a coulomb repulsion of $U = 17.3\Gamma_1$ at both dots and a cut-off energy $D = 2U = 34.6\Gamma_1$. The spacing between the nearest energy levels is assumed to be higher

than D , hence only one level is relevant in dynamics of the system. Particle-Hole-Symmetry at each dot is obtained when $\epsilon_i = \frac{U}{2}$. At this point, there is an odd number of electrons at each dot. Hence, at sufficiently low temperature the system will exhibit the characteristic Kondo peak Wilson²¹. Observing how the Kondo-effect interacts with the Majorana signature in the double quantum dot is also an insight of this project.

To improve the efficiency of the code we took advantage of the preserved symmetries: The spin- \uparrow particle number \hat{N}_\uparrow and the spin- \downarrow parity $\hat{P}_\downarrow = \pm$ (+ even, - odd). The spin- \downarrow particle number is not preserved due to the majorana coupling⁶. The initial Hamiltonian organized in blocks according to these symmetries. This structure is preserved during the entire process. The spectral functions are then computed through the Density Matrix Renormalization Group (DM-NRG) approach²⁴.

III. RESULTS

A. Non-interacting dots

In non-interacting dots ($U = 0$), the density of states at each dot can be obtained from equation (9) by replacing the green function at 7. The manipulation of the Majorana mode is achieved by tuning the model parameters ($t_1, t_2, \epsilon_1, \epsilon_2, t_{dots}$). Two types of majorana signatures are observed.

- **Type I:** The spin- \downarrow DOS is the half of the spin- \uparrow DOS at the Fermi energy ($\rho_\downarrow(0) = \rho_\uparrow(0)$).
- **Type II:** The spin- \downarrow Fermi energy is equal about 5.2. This is the value such that $\pi\Gamma_1\rho_\downarrow(0) = 0.5$, characteristic of a decay of half a quanta in the conductivity.

B. Manipulation in non-interacting QDs

C. Manipulation in interacting QDs

IV. CONCLUDING REMARKS

Conclusion goes here.

ACKNOWLEDGMENTS

The authors thank Edson Vernek for enlightening discussions. L.G.G.V.D.S. acknowledges financial support by CNPq (grants No. 307107/2013-2 and 449148/2014-9), and FAPESP (grant No. 2016/18495-4).

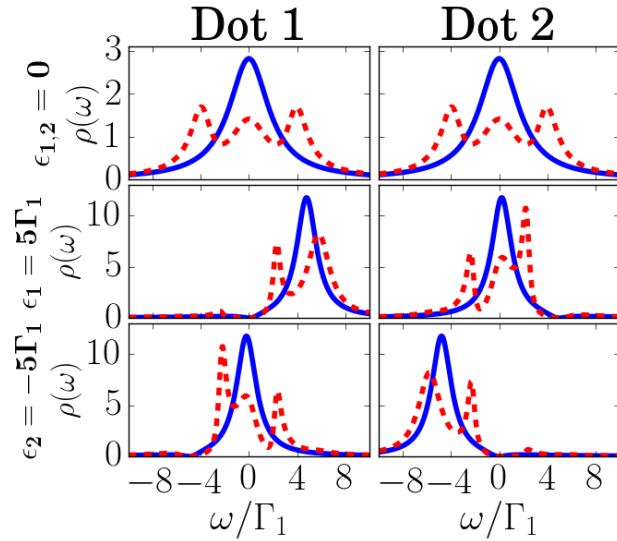


FIG. 3: DQD-Majorana set-up. Solid lines: standard coupling. Dashed lines: Majorana spin- \downarrow effective couplings (6). The atomic energy levels appear inside each QD. Red dashed horizontal lines represent the Fermi level.

- ¹ A. Y. Kitaev, *Physics-Uspekhi* **44**, 131 (2001).
- ² V. Mourik, K. Zuo, S. M. Frolov, S. R. Plissard, E. P. a. M. Bakkers, and L. P. Kouwenhoven, *Science* **336**, 1003 (2012).
- ³ A. Das, Y. Ronen, Y. Most, Y. Oreg, M. Heiblum, and H. Shtrikman, *Nature Physics* **8**, 887 (2012).
- ⁴ M. T. Deng, C. L. Yu, G. Y. Huang, M. Larsson, P. Caroff, and H. Q. Xu, *Nano Letters* **12**, 6414 (2012).
- ⁵ H. Zhang, C.-X. Liu, S. Gazibegovic, D. Xu, J. A. Logan, G. Wang, N. van Looy, J. D. S. Bommer, M. W. A. de Moor, D. Car, R. L. M. Op het Veld, P. J. van Veldhoven, S. Koelling, M. A. Verheijen, M. Pendharkar, D. J. Pennachio, B. Shojaei, J. S. Lee, C. J. Palmstrm, E. P. A. M. Bakkers, S. D. Sarma, and L. P. Kouwenhoven, *Nature* **556**, 74 (2018).
- ⁶ A. Y. Kitaev, *Annals of Physics* **303**, 2 (2003), arXiv: quant-ph/9707021.
- ⁷ S. D. Sarma, M. Freedman, and C. Nayak, *npj Quantum Information* **1**, 15001 (2015).
- ⁸ D. E. Liu and H. U. Baranger, *Physical Review B* **84** (2011), 10.1103/PhysRevB.84.201308, arXiv: 1107.4338.
- ⁹ E. Vernek, P. H. Penteado, A. C. Seridonio, and J. C. Egues, *Physical Review B* **89**, 165314 (2014).
- ¹⁰ M. T. Deng, S. Vaitiekenas, E. B. Hansen, J. Danon, M. Leijnse, K. Flensberg, J. Nygard, P. Krogstrup, and C. M. Marcus, *Science* **354**, 1557 (2016).
- ¹¹ M. Lee, J. S. Lim, and R. Lopez, *Physical Review B* **87**, 241402 (2013).
- ¹² D. A. Ruiz-Tijerina, E. Vernek, L. G. G. V. Dias da Silva, and J. C. Egues, *Physical Review B* **91**, 115435 (2015).
- ¹³ M. Barkeshli and J. D. Sau, [arXiv:1509.07135 \[cond-mat, physics:quant-ph\]](#) (2015), arXiv: 1509.07135.
- ¹⁴ T. Karzig, C. Knapp, R. M. Lutchyn, P. Bonderson, M. B. Hastings, C. Nayak, J. Alicea, K. Flensberg, S. Plugge, Y. Oreg, C. M. Marcus, and M. H. Freedman, *Physical Review B* **95**, 235305 (2017).
- ¹⁵ M. A. Ruderman and C. Kittel, *Physical Review* **96**, 99 (1954).
- ¹⁶ T. Kasuya, *Progress of Theoretical Physics* **16**, 45 (1956).
- ¹⁷ K. Yosida, *Physical Review* **106**, 893 (1957).
- ¹⁸ L. G. G. V. Dias da Silva, N. Sandler, K. Ingersent, and S. E. Ulloa, *Physica E: Low-dimensional Systems and Nanostructures* **40**, 1002 (2008).
- ¹⁹ D. N. Zubarev, *Soviet Physics Uspekhi* **3**, 320 (1960).
- ²⁰ D. A. Spielman, *Algorithms, Graph Theory, and Linear Equations in Laplacian Matrices*, Proceedings of the International Congress of Mathematicians (2010).
- ²¹ K. G. Wilson, *Reviews of Modern Physics* **47**, 773 (1975).
- ²² M. Sindel, *Numerical Renormalization Group studies of Quantum Impurity Models in the Strong Coupling Limit*, Text.PhDThesis, Ludwig-Maximilians-Universitt Mnchen (2005).
- ²³ R. Bulla, T. A. Costi, and T. Pruschke, *Reviews of Modern Physics* **80**, 395 (2008).
- ²⁴ W. Hofstetter, *Physical Review Letters* **85**, 1508 (2000).

Appendix A: Computation of the Green Function

In Zubarev's fermionic ballistic transport approach¹⁹ the green functions associated to two operators $A(t)$,

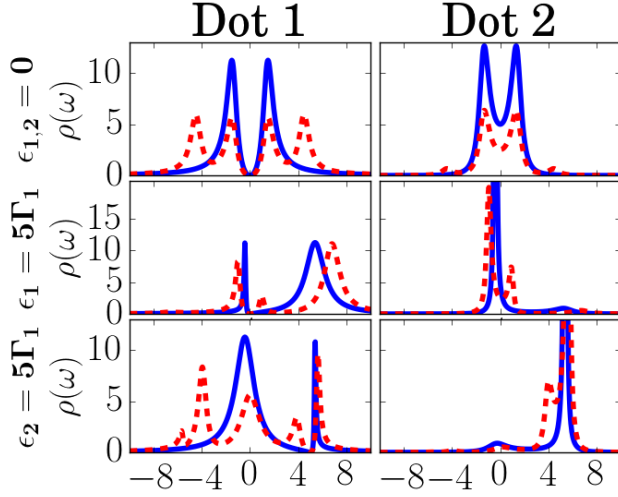


FIG. 4: DQD-Majorana set-up. Solid lines: standard coupling. Dashed lines: Majorana spin- \downarrow effective couplings (6). The atomic energy levels appear inside each QD. Red dashed horizontal lines represent the Fermi level.

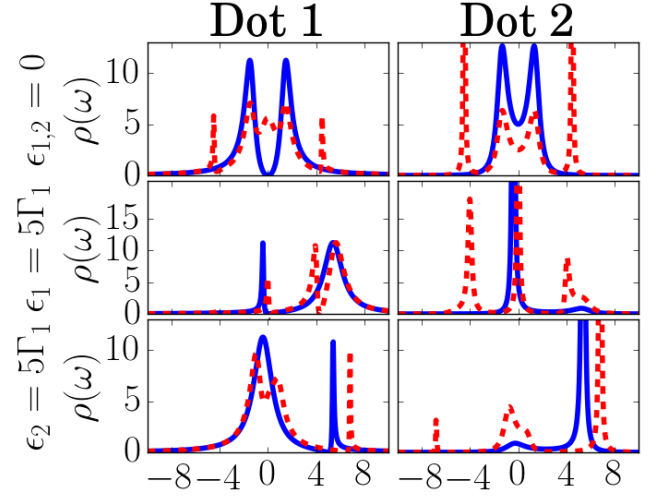


FIG. 5: DQD-Majorana set-up. Solid lines: standard coupling. Dashed lines: Majorana spin- \downarrow effective couplings (6). The atomic energy levels appear inside each QD. Red dashed horizontal lines represent the Fermi level.

$B(t)$ is defined as that Fourier transform of the time-ordered anti-commutator of A and B

$$G_{A,B}(\omega) = \mathcal{F} \{ \mathcal{T} [\{ A(t), B(t') \}] \} (\omega). \quad (\text{A1})$$

The Fourier transform of Schrodinger evolution determines the transport equations

$$\omega G_{A,B}(\omega) = \delta_{A^\dagger, B} + G_{[A,H],B}(\omega). \quad (\text{A2})$$

We can apply this to Hamiltonian (1) by replacing A and B by the creation and annihilation operators. To simplify the complexity of the system we fix $B = d_{1\downarrow}^\dagger$. In addition note that the transport equations for f_\downarrow and f_\downarrow^\dagger are

$$(\omega - \epsilon_M) G_{f_\downarrow, d_{1\downarrow}^\dagger}(\omega) = \frac{t}{\sqrt{2}} \left(G_{d_{1\downarrow}, d_{1\downarrow}^\dagger}(\omega) - G_{d_{1\downarrow}^\dagger, d_{1\downarrow}}(\omega) \right) \quad (\text{A3})$$

$$(\omega + \epsilon_M) G_{f_\downarrow^\dagger, d_{1\downarrow}^\dagger}(\omega) = \frac{t}{\sqrt{2}} \left(G_{d_{1\downarrow}, d_{1\downarrow}^\dagger}(\omega) - G_{d_{1\downarrow}^\dagger, d_{1\downarrow}}(\omega) \right), \quad (\text{A4})$$

which allows us to take $G_{f_\downarrow^\dagger, d_{1\downarrow}^\dagger}(\omega) = \frac{\omega + \epsilon}{\omega - \epsilon} G_{f_\downarrow, d_{1\downarrow}^\dagger}(\omega)$. Therefore, we can eliminate $G_{f_\downarrow^\dagger, d_{1\downarrow}^\dagger}(\omega)$ from the equations even before we start Gauss-Jordan process.

Writing the other equations we obtain the linear system

$$T \vec{G}_{d_1^\dagger} = \vec{e}_1 \quad (\text{A5})$$

where T is the transport matrix

$$\begin{bmatrix} \omega - \epsilon_1 & -V_1^* & -t_{dots} & \frac{-t_1}{\sqrt{2}} & 0 & 0 & 0 \\ -V_1 & \omega - \epsilon_k & -V_2 & 0 & 0 & 0 & 0 \\ -t_{dots}^* & -V_2^* & \omega - \epsilon_2 & \frac{-t_2}{\sqrt{2}} & 0 & 0 & 0 \\ \frac{-\sqrt{2}t_1^*}{\omega + \epsilon_M} & 0 & \frac{-\sqrt{2}t_2^*}{\omega + \epsilon_M} & \omega - \epsilon_M & \frac{\sqrt{2}t_2^*}{\omega + \epsilon_M} & 0 & \frac{\sqrt{2}t_1^*}{\omega + \epsilon_M} \\ 0 & 0 & 0 & \frac{t_2}{\sqrt{2}} & \omega + \epsilon_2 & V_2^* & t_{dots}^* \\ 0 & 0 & 0 & 0 & V_2 & \omega + \epsilon_k & V_1 \\ 0 & 0 & 0 & \frac{t_1}{\sqrt{2}} & t_{dots} & V_1^* & \omega + \epsilon_1 \end{bmatrix}, \quad (\text{A6})$$

$\vec{G}_{d_1^\dagger}$ is the column vector

$$[G_{d_{1\downarrow}, d_{1\downarrow}^\dagger}(\omega), G_{c_{k\downarrow}, d_{1\downarrow}^\dagger}(\omega), G_{d_{2\downarrow}, d_{1\downarrow}^\dagger}(\omega), G_{f_\downarrow, d_{1\downarrow}^\dagger}(\omega), G_{d_{2\downarrow}^\dagger, d_{1\downarrow}^\dagger}(\omega), G_{c_{k\downarrow}^\dagger, d_{1\downarrow}^\dagger}(\omega), G_{d_{1\downarrow}^\dagger, d_{1\downarrow}}(\omega)]^T$$

and \vec{e}_1 is the vector with entries $\hat{e}_{1n} = \delta_{1n}$.

The graph associated to this matrix is the one in FIG. 2. The energies inside each vertex are given by subtracting the corresponding diagonal term from ω . The couplings are just the negative of the off-diagonal terms.

1. The double quantum dot

To explain the process of Gaussian elimination we will obtain the green function for the case without Majorana fermion ($t_1 = t_2 = 0$). The transport matrix for this

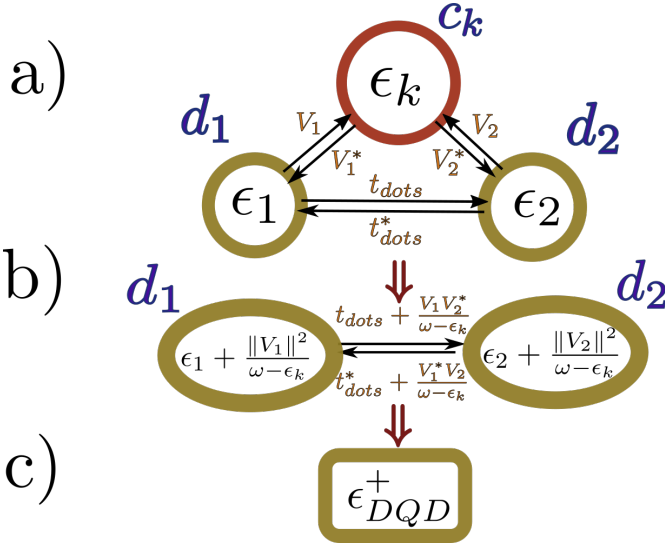


FIG. 6

system is

$$\begin{bmatrix} \omega - \epsilon_1 & -V_1 & -t_{dots} \\ -V_1^* & \omega - \epsilon_k & -V_2 \\ -t_{dots}^* & -V_2^* & \omega - \epsilon_2 \end{bmatrix}. \quad (\text{A7})$$

The graph associated to this matrix can be observed in FIG.6.a). To eliminate the vertex c_k we just need to subtract from (A7) the rank-1 matrix that cancels the row and the column corresponding to c_k . This matrix is

$$\begin{bmatrix} \frac{V_1^* V_1}{\omega - \epsilon_k} & -V_1^* & \frac{V_2 V_1^*}{\omega - \epsilon_k} \\ -V_1 & \omega - \epsilon_k & -V_2 \\ \frac{V_2^* V_1}{\omega - \epsilon_k} & -V_2^* & \frac{V_2^* V_2}{\omega - \epsilon_k} \end{bmatrix}. \quad (\text{A8})$$

The result of (A7) - (A8) is

$$\begin{bmatrix} \omega - \epsilon_1 - \frac{V_1^* V_1}{\omega - \epsilon_k} & 0 & -t_{dots} - \frac{V_2 V_1^*}{\omega - \epsilon_k} \\ 0 & 0 & 0 \\ -t_{dots}^* - \frac{V_2^* V_1}{\omega - \epsilon_k} & 0 & \omega - \epsilon_2 - \frac{V_2^* V_2}{\omega - \epsilon_k} \end{bmatrix} \quad (\text{A9})$$

which is depicted by the graphs in FIG.6.b). The next step is to pop-out the vertex d_2 following the same procedure. At the end, the energy inside the vertex d_1 will be

$$\epsilon_{DQD}^+ = \epsilon_1 + \sum_{\mathbf{k}} \frac{V_1 V_1^*}{\omega - \epsilon_{\mathbf{k}}} + \frac{\left\| t_{dots} + \sum_{\mathbf{k}} \frac{V_1 V_2^*}{\omega - \epsilon_{\mathbf{k}}} \right\|^2}{\omega - \epsilon_2 - \sum_{\mathbf{k}} \frac{V_2 V_2^*}{\omega - \epsilon_{\mathbf{k}}}} \quad (\text{A10})$$

and the green function of $G_{d_1 d_1^\dagger}(\omega)$ in a DQD will be given by $\frac{1}{\omega - \epsilon_{DQD}^+}$ (see FIG.6.c)).

2. Solution of the transport equations

The previous procedure can be generalized into the following algorithm:

1. To compute the transport equations with the second term fixed in the creation operator of the dot.
2. To set up the graph associated to the transport system.
3. To pop out the vertexes of the graph. Each pop-out process carries the following steps.
 - (a) To compute the extra-terms in the energies and couplings based on the walks passing through the vertex that will be popped out.
 - (b) To eliminate this vertex from the graph.
 - (c) To iterate till there is just one vertex.
4. To invert the last energy to obtain the final green function of the dot.

To solve the general case we start with the graph in FIG.2 and we pop out the vertexes $c_k, c_k^\dagger, d_{2,\downarrow}$ and $d_{2,\downarrow}^\dagger$ in that order. The energies associated to $d_{1,\downarrow}$ and $d_{1,\downarrow}^\dagger$ will be similar to (A10) giving

$$\epsilon_{DQD}^\pm = \pm \epsilon_1 + \sum_{\mathbf{k}} \frac{V_1 V_1^*}{\omega - \epsilon_{\mathbf{k}}} + \frac{\left\| \pm t_{dots} + \sum_{\mathbf{k}} \frac{V_1 V_2^*}{\omega - \epsilon_{\mathbf{k}}} \right\|^2}{\omega \pm \epsilon_2 - \sum_{\mathbf{k}} \frac{V_2 V_2^*}{\omega - \epsilon_{\mathbf{k}}}}. \quad (\text{A11})$$

There is also a correction in the couplings between the Majorana mode and $d_{1,\downarrow}, d_{1,\downarrow}^\dagger$ given by

$$T_\pm = \pm t_1 \pm t_2 \frac{\left(\pm t_{dots} + \sum_{\mathbf{k}} \frac{V_1 V_2^*}{\omega - \epsilon_{\mathbf{k}}} \right)}{\omega \pm \epsilon_2 \pm \sum_{\mathbf{k}} \frac{V_2 V_2^*}{\omega - \epsilon_{\mathbf{k}}}}. \quad (\text{A12})$$

Finally since the Majorana is in contact with dot 2, there is an extra-term appearing in the Majorana energy given by

$$\epsilon_{M2} = \omega - \epsilon_M - \frac{\frac{\omega}{\omega + \epsilon_M} \|t_2\|^2}{\omega - \epsilon_2 - \sum_{\mathbf{k}} \frac{V_2 V_2^*}{\omega - \epsilon_{\mathbf{k}}}} - \frac{\frac{\omega}{\omega + \epsilon_M} \|t_2\|^2}{\omega + \epsilon_2 - \sum_{\mathbf{k}} \frac{V_2 V_2^*}{\omega + \epsilon_{\mathbf{k}}}}. \quad (\text{A13})$$

With all the terms of the graph in FIG.2.b) computed, it only remains to pop out vertexes d_1^\dagger and f_\downarrow in that order to obtain the green function in equation (7).